Applied Physics Letters

Controllable finite ultra-narrow quality-factor peak in a perturbed Dirac-cone band structure of a photonic-crystal slab

Cite as: Appl. Phys. Lett. **119**, 031105 (2021); https://doi.org/10.1063/5.0056243
Submitted: 07 May 2021 • Accepted: 06 July 2021 • Published Online: 19 July 2021

Alex Y. Song, Akhil Raj Kumar Kalapala, Ricky Gibson, et al.

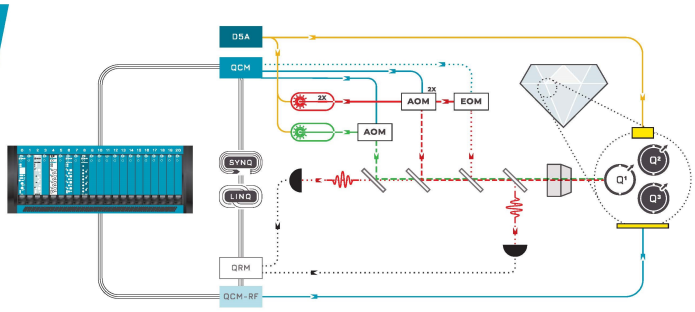

Applied Physics Letters ARTICLE scitation.org/journal/apl

Controllable finite ultra-narrow quality-factor peak in a perturbed Dirac-cone band structure of a photonic-crystal slab

Cite as: Appl. Phys. Lett. **119**, 031105 (2021); doi: 10.1063/5.0056243
Submitted: 7 May 2021 · Accepted: 6 July 2021 ·
Published Online: 19 July 2021

View Online Export Citation CrossMark

Alex Y. Song,[1] Akhil Raj Kumar Kalapala,[2] Ricky Gibson,[3] Kevin James Reilly,[4] Thomas Rotter,[4] Sadhvikas Addamane,[4] Haiwen Wang,[5] Cheng Guo,[5] Ganesh Balakrishnan,[4] Robert Bedford,[3] Weidong Zhou,[2] and Shanhui Fan[1,a)]

AFFILIATIONS

[1]Department of Electrical Engineering, Stanford University, Stanford, California 94305, USA
[2]Department of Electrical Engineering, University of Texas at Arlington, Arlington, Texas 76019, USA
[3]Air Force Research Laboratory, Wright-Patterson AFB, Dayton, Ohio 45433, USA
[4]Department of Electrical and Computer Engineering, University of New Mexico, Albuquerque, New Mexico 87131, USA
[5]Department of Applied Physics, Stanford University, Stanford, California 94305, USA

Note: This paper is part of the APL Special Collection on Zero-index Metamaterials for Classical and Quantum Light.
[a)]**Author to whom correspondence should be addressed:** shanhui@stanford.edu

ABSTRACT

We show that by using a perturbed photonic Dirac-cone, one can realize an ultra-narrow and finite Q-factor peak in the wavevector space, with both the peak value and the width separately tunable. We also discuss a lower bound in the minimal viable width given a peak Q-value while maintaining sufficient Q differentiation among modes. The strong angular and frequency Q-selection finds applications in optical devices where strong angle- and frequency-selections are needed.

Engineering the photonic band structure has led to significant advances in the development of optoelectronic devices.[1–3] Most band structure engineering focuses on the eigenfrequency of the modes as a function of the wavevector. Recently, on the other hand, engineering the quality-factor (Q-factor) as a function of the wavevector has drawn increasing interest due to a number of applications such as light-trapping, two-dimensional lasing, and meta optics.[4–12] One of the desired features in such engineering is to obtain a fully controllable *finite* and *narrow* high-Q peak. This allows the devices to interact with the electromagnetic waves only at a certain angle and frequency, which is important in angle-selective optical devices such as absorbers[13–24] and thermal emitters.[16,25–37] This feature is also useful in achieving single-mode large-area lasing for high-power applications. Such devices have always been challenging since as the device-size scales, the spacing between the modes in the wavevector space reduces, leading to a diminishing Q-difference and, hence, threshold-difference.[38–42]

By exploring a perturbed photonic Dirac-cone,[43–45] in this Letter, we demonstrate an ultra-narrow finite Q peak in a photonic-crystal slab. Both the peak Q-factor and its width in the wavevector space are independently controllable. Our approach exploits the strong mixing between the Dirac-cone bands to the linear order in the wavevector. Such mixing leads to a drastic Q reduction away from the Brillouin zone center Γ. The peak Q can be tuned by the strength of the perturbation, i.e., the size of the additional small holes in the photonic-crystal slab. The width of the peak can be tuned by the thickness of the slab. We also derive a trade-off relation between the peak Q value and the width, which gives a lower bound of the latter given the former. Our construction can be used to fabricate perfect absorbers that are both direction- and frequency-selective. The design of surface-emitting lasers can also benefit from this result, as a controllable outstanding high-Q mode at Γ promotes single-mode lasing in a scaled device.

To motivate our results, we consider generically how a peaked Q can be obtained. In the following, we examine optical resonators with a light incident or output in the out-of-plane direction, with $\boldsymbol{k} = (k_x, k_y)$ representing the 2D in-plane wavevector, as illustrated in Fig. 1. Our goal is to obtain a peaked Q as a function of the angles. We start with a uniform dielectric slab, which can be found in vertical-cavity surface-emitting

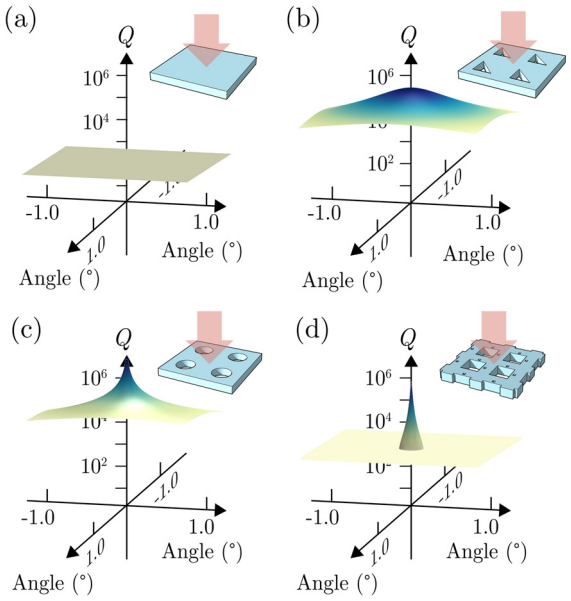

FIG. 1. Comparison of the angular Q variation in different structures. (a) A Fabry–Pérot band at the frequency of $0.5\,c/d$ in a uniform slab of thickness d and permittivity of 12, where c is the light speed. (b) A guided resonance mode at the frequency of $0.36\,c/l$ in a photonic-crystal slab, where l is the periodicity of the photonic-crystal. The slab has a thickness of $0.8\,l$. The side length of the isosceles right triangle holes is $0.5\,l$. (c) A guided resonance mode at the frequency of $0.49\,c/l$ in a photonic-crystal slab containing circular holes. The slab has a thickness of $0.5\,l$, whereas the radius of the holes is $0.2\,l$. (d) The quadrupole band for the perturbed photonic-crystal slab structure shown in Fig. 2.

lasers (VCSELs). There are Fabry–Pérot resonances in the vertical direction in the slab. Their Q-factors as a function of the wave incident angle are nearly constant near the normal direction, as shown in Fig. 1(a). This can be improved by introducing a 2D photonic crystal in the slab, as illustrated in Fig. 1(b). Here, the modes at the non-zero angles have a lower Q than the mode at the normal direction, i.e., the Brillouin zone center Γ. When used in a photonic-crystal surface-emitting laser (PCSEL), the mode at Γ would exhibit a lower threshold than other modes. This is in accordance with the recent success of PCSELs, where single-mode lasing is maintained in a much larger area compared to the VCSELs.[8,41,42] Such a peaked $Q(\boldsymbol{k})$ function can be viewed as a result of a quasi-bound states in the continuum (quasi-BIC).[9] The $Q(\boldsymbol{k})$ function of a band containing a symmetry-protected BIC at Γ is plotted in Fig. 1(c). This is a singly degenerate band in a photonic-crystal slab with circular holes in each unit-cell. Due to the D_{4h} symmetry, the mode at Γ cannot couple to free-space radiation. When the symmetry is broken such as by using triangular holes, the mode at Γ may acquire a finite Q such as the one shown in Fig. 1(b). Typically, this process leads to a high-Q band in the vicinity of Γ, as is observed in Figs. 1(b) and 1(c).

Our task here is to further narrow the $Q(\boldsymbol{k})$ peak to such as the one shown in Fig. 1(d), where high-Q (e.g., $>10^5$) only exists in a narrow $\boldsymbol{k}$ region, and the band becomes low-Q outside. Our design concept is as follows. In a photonic-crystal slab, there exist some high-Q modes and low-Q modes at Γ. We can further assume that some modes have different symmetries at Γ, such that they will not mix, and moreover, it is possible to tune the structure so that the real part of the frequency of these modes is degenerate. At a non-zero $\boldsymbol{k}$, since the symmetry is lowered from Γ, these modes start to mix with each other. Generically, such a mixing leads to a high-Q peak at Γ. The width of the peak is controlled by the strength of the $\boldsymbol{k}\cdot\boldsymbol{p}$ terms that mix the modes.[45] At small $\boldsymbol{k}$, the strongest possible such term is to the linear order in $\boldsymbol{k}$. If we consider a high-Q mode $|q\rangle$ and a low-Q mode $|d\rangle$ at Γ, generically, the narrowest Q peak should be described by the following effective $\boldsymbol{k}\cdot\boldsymbol{p}$ Hamiltonian:

$$h(k) = \begin{pmatrix} i\gamma_d & iv_g k \\ -iv_g k & i\gamma_q \end{pmatrix}, \tag{1}$$

along a direction $\boldsymbol{k}$ in the Brillouin zone. Here, $k = |\boldsymbol{k}|$ is the magnitude of the in-plane wavevector, v_g is the group velocity of the bands, γ_d is the radiation constant of the low-Q mode at Γ, and γ_q is that of the high-Q mode at Γ. The resulting $Q(\boldsymbol{k})$ function for the band containing mode $|q\rangle$ is plotted in Fig. 1(d), assuming the parameters of $\gamma_q = 6.7\times10^{-7}$, $\gamma_d = 3.8\times10^{-4}$, and $v_g = 0.11\,c/2\pi$. Due to the strong mixing that is linear in $\boldsymbol{k}$, the Q factor reduces drastically away from Γ, leading to a finite and narrow Q peak.

The remaining task is to design a structure that gives the effective Hamiltonian in Eq. (1). The linear mixing in Eq. (1) corresponds to a Dirac-cone band structure.[43,44] In a photonic crystal slab, one can form a Dirac cone by creating an accidental degeneracy at the Γ point between a pair of twofold degenerate dipole states and a singly degenerate state.[43,44,46] However, in these previous works, due to the symmetry of the structure used, the singly degenerate state has an infinite Q. The resulting system, thus, does not have the desired $Q(\boldsymbol{k})$ dependency.[45] Our approach is to start with a Dirac-cone formed by the approach described above and perturb it such that the infinite-Q mode becomes radiative.

To implement our approach, we consider the photonic-crystal slab structure, as is shown in the inset of Fig. 2(a). The photonic-crystal slab has a square lattice with period l in both x and y directions. We normalize all the other geometrical parameters in units of l. The slab has a thickness of $t = 0.8\,l$ and a permittivity of 12, as is typical for common semiconductors in the infrared wavelength range.

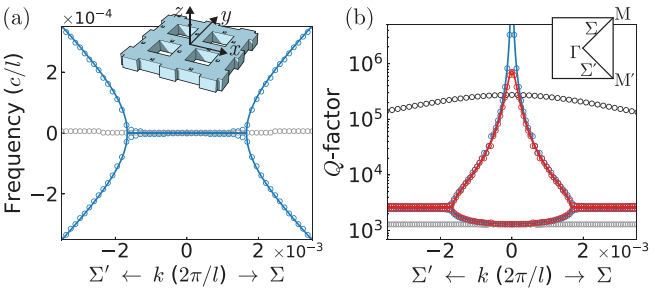

FIG. 2. Band structure and the $Q(\boldsymbol{k})$ function of the photonic Dirac-cone. Circles represent numerical calculation results, while solid curves represent results of the effective model in Eq. (1). (a) Band structure of the unperturbed structure. Two dispersive (blue) bands and the flatband (gray) are plotted. Inset: schematic of the photonic-crystal slab. The frequency is offset to the Dirac-cone frequency at $0.496\,c/l$. (b) $Q(\boldsymbol{k})$ functions of the unperturbed structure (blue) and the perturbed (red). The flatband is plotted in gray circles. Black circles represent the $Q(\boldsymbol{k})$ function of the photonic-crystal slab with triangular holes. Inset: diagram of the first Brillouin zone.

In each unit-cell, there is a large square-shaped hole at the center with a side length of a_1 and two smaller holes with a side length of $a_2 = 0.05\,l$ located at $(0.4\,l, 0)$ and $(0, 0.4\,l)$, respectively. The large hole is through the slab, while the smaller holes have a depth of $t_2 = 0.05\,l$. In reality, for a device operating in the infrared wavelength range, the side length and the depth of the small holes would be on the order of 10's of nm, which is within the capabilities of state-of-the-art fabrication technique.[47] Without the smaller holes, the PhC slab has a D_{4h} point-group symmetry.[48] The symmetry reduces to C_{2v} with the smaller holes added.

The band structure and the $Q(\boldsymbol{k})$ functions can be directly calculated by monitoring the poles of the scattering matrix on the complex frequency plane.[49] The results are plotted as blue circles in Figs. 2(a) and 2(b). In the absence of the smaller holes and with a side length of $a_1 = 0.69\,l$, three modes are tuned to degeneracy at Γ. In the resulting band structure in Fig. 2, two of the bands are dispersive, while the third forms a flatband. Both the band structure in Fig. 2(a) and the $Q(\boldsymbol{k})$ functions in Fig. 2(b) show two phases separated by exceptional points.[44] At Γ, the infinite-Q mode belongs to the B_{1g} representation of the D_{4h} point group and is of quadrupole nature. The low-Q mode belongs to the E_u representation, which is of dipolar nature and strongly couples to free-space radiation. The resulting $Q(\boldsymbol{k})$ is sharply peaked for one of the bands. However, the mode at Γ in this band has an infinite Q-factor and is a bound state in the continuum (BIC),[5] which cannot couple to free space to perform light detection, absorption, or emission.

To create a sharply peaked $Q(\boldsymbol{k})$, where Q is finite at the peak, we perturb the structure by introducing two smaller holes as mentioned above to break the D_{4h} symmetry, such that the quadrupole mode is allowed to radiate. With the perturbation, the real part of the band structure is virtually identical to the one without in Fig. 2(a), hence is not plotted. The $Q(\boldsymbol{k})$ functions with the perturbation are shown as red circles in Fig. 2(b). We observe that the $Q(\boldsymbol{k})$ functions for both the high-Q and the low-Q bands are very close to those without perturbation, except near the Brillouin zone center Γ. At Γ, the high-Q mode now has a finite Q-factor rather than infinite. Away from Γ, the Q-factor quickly reduces, thus, forming a sharp peak at Γ. As a reference, the $Q(\boldsymbol{k})$ function of the band at the frequency of $0.36\,c/l$ in a photonic-crystal slab with a square lattice and triangular holes is also plotted in the black curve in Fig. 2(b).[8,49] This is a singly degenerate band with no other bands nearby in frequency; hence, it does not form a Dirac-cone. A schematic of this structure can be found in Fig. 1(b). The peak Q-factor is at a level of 10^5, similar to our design here. However, the $Q(\boldsymbol{k})$ function is much more slowly varying. The Q peak width is reduced by an order of magnitude in our work through exploiting the strong linear-order mixing.

The band structure and the $Q(\boldsymbol{k})$ function of the two dispersive bands are described by the effective Hamiltonian in Eq. (1).[44] Here, γ_d and γ_q can be readout from the numerical calculations at the Brillouin zone center Γ. v_g can be obtained by fitting to the slope of the bands outside the exceptional points. The complex eigenfrequencies of the Dirac-cone bands are then obtained by solving Eq. (1). The resulting band structure and the $Q(\boldsymbol{k})$ functions are plotted as solid curves in Fig. 2. The results very accurately reproduce the numerical simulations. In existing studies of the photonic Dirac-cones, γ_q is zero, leading to an infinite Q-factor. In our work, γ_q becomes finite due to the introduction of the smaller holes. The perturbation can also cause small corrections to other parameters in Eq. 1, which are omitted in the lowest order. From Eq. (1), it is clear that the off diagonal terms that are linear in $\boldsymbol{k}$ cause a strong mixing between the dipolar and the quadrupole modes, resulting in a sharp Q peak. It is important to note that the entire band structure and the $Q(\boldsymbol{k})$ functions are controlled by only three parameters, i.e., γ_d, γ_q, and v_g.

In our approach to engineer the $Q(\boldsymbol{k})$ function, both the peak Q and its width can be tuned. The peak Q value can be straightforwardly engineered by controlling the size of the small holes. For example, in Fig. 3(a), we plot the $Q(\boldsymbol{k})$ function of the same structure as above, but with the small holes having a reduced side length and depth of $a_2 = t_2 = 0.04\,l$. The resulting Q-factor at Γ now increases by a factor of 5, while the width of the peak remains largely unchanged. We also note that here we have changed both the side length a_2 and the depth t_2 of the small holes, and that the small holes are added only to one side of the slab. In such a scenario, the definition of the asymmetry factor as found in Ref. 9 is a question of interest, but will not be a focus of this work.

To tune the width of the Q peak without changing the peak value, we can change the Q-factor of the dipolar mode at Γ. As discussed above, the $Q(\boldsymbol{k})$ functions of both bands are controlled by only three parameters, i.e., γ_q, γ_d, and v_g. By increasing the Q-factor of the dipolar mode, the region inside the exceptional points shrinks, leading to a reduced peak width. A demonstration is shown in Fig. 3(b), in which we compare the $Q(\boldsymbol{k})$ function of the design above that corresponds to the red curve in Fig. 3(a) and one with a reduced slab thickness of $t = 0.775\,l$ (purple). The side length of the large hole is adjusted to $0.695\,l$ to maintain the degeneracy of the real part of the bands. We also tune the smaller holes to have a side length and depth of $a_2 = t_2 = 0.035\,l$ to maintain the peak Q-value at Γ. The resulting $Q(\boldsymbol{k})$ functions of both numerical calculation (circles) and the analytical model (solid curves) are shown. The Q-factor of the dipolar mode increased by four times in the thinner photonic-crystal slab. As a result, the high-Q bandwidth reduces by a factor of 2, while the peak Q value is unchanged, as is observed in Fig. 3(b).

We note that even without adding the perturbation, in practice, a finite-sized device or experimental imperfections would also lead to a finite Q-factor at Γ. However, the resulting Q peak value and its width are not fully controllable.

The above discussion of the tuning of the high-Q width gives a hint of a relation between the minimal viable width and the peak Q.

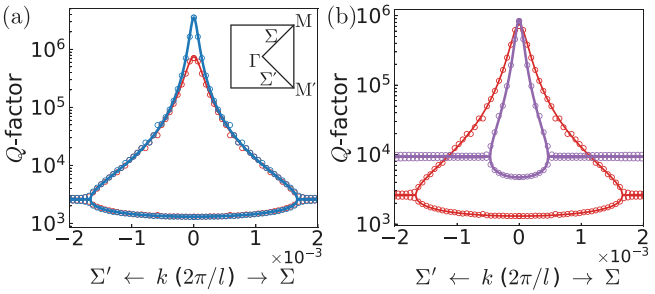

FIG. 3. (a) The $Q(\boldsymbol{k})$ functions of the photonic-crystal slab with the side length and depth of the small holes to be $0.05\,l$ (red) and $0.04\,l$ (blue), respectively. (b) The $Q(\boldsymbol{k})$ functions of the photonic-crystal slab with a thickness of $0.8\,l$ (red) and $0.775\,l$ (purple), respectively. The circles are results of the numerical calculation. The solid curves are results of the effective model in Eq. (1).

In real devices, it is often desirable to design a certain Q-factor at the zone center Γ, and at the same time, a strong Q-differentiation against other modes is away from Γ. For simplicity, we define the width of the high-Q region by the width of the wavevector region inside the exceptional points. The location of the exceptional point can be calculated from Eq. (1) as $k_e = (\gamma_d - \gamma_q)/2v_g$. It is clear that a higher Q_d, i.e., a smaller γ_d, leads to a smaller k_e. By the requirement of Q-differentiation, we consider that the peak Q value at Γ is at least twice the value outside the exceptional points. The minimal γ_d is then given by $\gamma_d = 3\gamma_q$. This leads to a minimal width as

$$w_{\min} = 2k_e = 2\frac{\omega}{Q_{\max} \cdot v_g}, \tag{2}$$

where ω is the frequency of the Dirac point, Q_{max} is the desired peak quality factor at Γ, and v_g is the group velocity of the Dirac-cone bands. For a target Q-factor at Γ, Eq. (2), thus, gives the lower bound on the minimal peak width while maintaining sufficient Q differential from the Γ point to other wave vectors.

A sharply peaked $Q(\boldsymbol{k})$ function is useful in a variety of scenarios where strong angle- and frequency-differentiation is needed, such as angle-selective sensors or large-area single-mode lasers. As an example, here, we demonstrate a perfect absorber based on the photonic-crystal slab with a strong selection in both the frequency and the incident angle. The geometric parameters of the slab are as follows. The slab has a thickness of $t = 0.85\,l$, the large hole has a side length of $0.682\,l$, and the small holes have a depth and a side length of $0.1\,l$. We add a mirror to the bottom of the photonic-crystal slab at a distance of $20.3\,l$. The bottom mirror eliminates the radiation channels in the bottom, enabling perfect absorption from one-sided incidence from the top. Light is incident from the top. We make use of the quadrupole mode at Γ, which is an outstanding high-Q point in a parameter space of three dimensions, i.e., frequency plus 2D solid angles. We assume a uniform material loss in the photonic-crystal slab by adding a constant imaginary part to its refractive index, i.e., $\varepsilon = 12 - 4.8 \times 10^{-5}i$, representing a semiconductor interband absorption that is typically much broader than the optical resonance. Such a material absorption provides a modal internal loss to the quadrupole mode at Γ in the same amount as the radiative loss and, hence, resulting in a perfect absorption due to critical coupling.[50,51] At any other angle or frequency, such condition is not met and the absorption is low. The numerical results are shown in Fig. 4, where light is incident onto the structure with varying frequencies and angles. Here, light is assumed to be polarized such that the in-plane projection of the electric field is pointed in the 45° direction, i.e., it is p-polarized for the spectra along Σ and s-polarized along Σ', set by the selection rule of the modes.[52] It is observed that strong absorption only occurs within an angle of 0.1° from normal, in a narrow frequency range of $10^{-5}\,c/l$. Again, the width of the angle can be tuned by changing the Q-factor of the dipolar mode, for example by tuning the slab thickness. We note that the adding of the bottom mirror can introduce a correction to the frequency and the radiative constant of both the dipolar and the quadrupole bands.[53] Yet, this would not affect the narrowing of the Q peak in the perturbed Dirac-cone.

In summary, in this Letter, we presented an approach to obtain a finite and ultra-narrow Q peak, with the peak value and width independently tunable. This is realized by employing a perturbed photonic Dirac-cone. Utilizing the linear mixing between modes in the Dirac-cone, the modes at Γ strongly remix away from Γ, leading to a rapidly decreasing $Q(\boldsymbol{k})$ function for a high-Q band. The narrow Q peak is useful in scenarios where angular selection is needed, such as directional absorber or emitter. The feature can be useful in surface-emitting lasers as well, since a large Q differentiation promotes single-mode lasing. Although we focus on the 2D PhC structure, this approach applies to other dimensions such as 1D-distributed Bragg reflectors (DBRs).

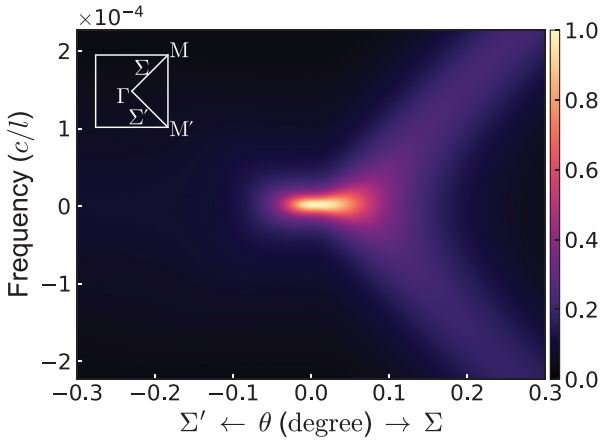

FIG. 4. The absorption spectra of the angle- and frequency-selective absorbers. The frequency is offset to the Dirac-cone point at 0.485 (c/l). The incident wave is polarized such that the in-plane projection of the electric field is pointed in the 45° direction.

See the supplementary material for (1) the detailed description of the calculation of the band structure using poles of the scattering matrix on a complex frequency plane, (2) the calculated band structure of the photonic-crystal slab in the inset of Fig. 2(a) in a larger frequency and wavevector range, and (3) the polynomial expansion of the $Q(\boldsymbol{k})$ function using its tuning parameters.

This work was supported in part by the Department of Defense Joint Directed Energy Transition Office (DE-JTO) under Grant No. N00014-17-1-2557.

DATA AVAILABILITY

The data that support the findings of this study are available from the corresponding author upon reasonable request.

REFERENCES

[1]K. Sakoda, *Optical Properties of Photonic Crystals* (Springer Science & Business Media, 2004), Vol. 80.
[2]J. D. Joannopoulos, S. G. Johnson, J. N. Winn, and R. D. Meade, *Photonic Crystals: Molding the Flow of Light*, 2nd ed. (Princeton University Press, 2008).
[3]W. L. Barnes, A. Dereux, and T. W. Ebbesen, "Surface plasmon subwavelength optics," Nature **424**, 824–830 (2003).
[4]J. Jin, X. Yin, L. Ni, M. Soljačić, B. Zhen, and C. Peng, "Topologically enabled ultrahigh-q guided resonances robust to out-of-plane scattering," Nature **574**, 501–504 (2019).
[5]C. W. Hsu, B. Zhen, A. D. Stone, J. D. Joannopoulos, and M. Soljačić, "Bound states in the continuum," Nat. Rev. Mater. **1**, 16048 (2016).

[6]A. Kodigala, T. Lepetit, Q. Gu, B. Bahari, Y. Fainman, and B. Kanté, "Lasing action from photonic bound states in continuum," Nature **541**, 196–199 (2017).
[7]M. I. Molina, A. E. Miroshnichenko, and Y. S. Kivshar, "Surface bound states in the continuum," Phys. Rev. Lett. **108**, 070401 (2012).
[8]K. Hirose, Y. Liang, Y. Kurosaka, A. Watanabe, T. Sugiyama, and S. Noda, "Watt-class high-power, high-beam-quality photonic-crystal lasers," Nat. Photonics **8**, 406–411 (2014).
[9]K. Koshelev, S. Lepeshov, M. Liu, A. Bogdanov, and Y. Kivshar, "Asymmetric metasurfaces with high-q resonances governed by bound states in the continuum," Phys. Rev. Lett. **121**, 193903 (2018).
[10]P. Bermel, C. Luo, L. Zeng, L. C. Kimerling, and J. D. Joannopoulos, "Improving thin-film crystalline silicon solar cell efficiencies with photonic crystals," Opt. Express **15**, 16986–17000 (2007).
[11]R. Singh, W. Cao, I. Al-Naib, L. Cong, W. Withayachumnankul, and W. Zhang, "Ultrasensitive terahertz sensing with high-q Fano resonances in metasurfaces," Appl. Phys. Lett. **105**, 171101 (2014).
[12]S. T. Ha, Y. H. Fu, N. K. Emani, Z. Pan, R. M. Bakker, R. Paniagua-Domínguez, and A. I. Kuznetsov, "Directional lasing in resonant semiconductor nanoantenna arrays," Nat. Nanotechnol. **13**, 1042–1047 (2018).
[13]Y. Takeda, T. Maruya, and H. Tanaka, "Absorptive angular-selective filters consisting of dielectric multilayers combined with thin absorbing layers," Appl. Opt. **58**, 9094 (2019).
[14]L. Zhu, F. Liu, H. Lin, J. Hu, Z. Yu, X. Wang, and S. Fan, "Angle-selective perfect absorption with two-dimensional materials," Light: Sci. Appl. **5**, e16052 (2016).
[15]Z. Zhou, E. Sakr, Y. Sun, and P. Bermel, "Solar thermophotovoltaics: Reshaping the solar spectrum," Nanophotonics **5**, 1–21 (2016).
[16]E. D. Kosten, J. H. Atwater, J. Parsons, A. Polman, and H. A. Atwater, "Highly efficient GaAs solar cells by limiting light emission angle," Light: Sci. Appl. **2**, e45–e45 (2013).
[17]C.-S. Hwang, S.-P. Yang, K.-W. Jang, J.-W. Park, and K.-H. Jeong, "Angle-selective optical filter for highly sensitive reflection photoplethysmogram," Biomed. Opt. Express **8**, 4361 (2017).
[18]S. Morita, H. Shiomi, H. Murata, and A. Sanada, "Highly angle and frequency selective absorption by mushroom metasurfaces for indoor propagation control," in *2017 IEEE MTT-S International Conference on Microwaves for Intelligent Mobility, ICMIM 2017* (IEEE, 2017), pp. 68–70.
[19]Y. Takeda, H. Iizuka, N. Yamada, and T. Ito, "Light trapping for photovoltaic cells using polarization-insensitive angle-selective filters under monochromatic illumination," Appl. Opt. **56**, 5761 (2017).
[20]B. H. Woo, I. C. Seo, E. Lee, S.-C. An, H. Y. Jeong, and Y. C. Jun, "Angle-dependent optical perfect absorption and enhanced photoluminescence in excitonic thin films," Opt. Express **25**, 28619 (2017).
[21]Y. Shen, D. Ye, I. Celanovic, S. G. Johnson, J. D. Joannopoulos, and M. Soljačić, "Optical broadband angular selectivity," Science **343**, 1499–1501 (2014).
[22]E. Sakr and P. Bermel, "Angle-selective reflective filters for exclusion of background thermal emission," Phys. Rev. Appl. **7**, 044020 (2017).
[23]R. E. Hamam, I. Celanovic, and M. Soljačić, "Angular photonic band gap," Phys. Rev. A **83**, 035806 (2011).
[24]J. R. Piper and S. Fan, "Total absorption in a graphene monolayer in the optical regime by critical coupling with a photonic crystal guided resonance," ACS Photonics **1**, 347–353 (2014).
[25]D. G. Baranov, Y. Xiao, I. A. Nechepurenko, A. Krasnok, A. Alù, and M. A. Kats, "Nanophotonic engineering of far-field thermal emitters," Nat. Mater. **18**, 920 (2019).
[26]D. Costantini, A. Lefebvre, A.-L. Coutrot, I. Moldovan-Doyen, J.-P. Hugonin, S. Boutami, F. Marquier, H. Benisty, and J.-J. Greffet, "Plasmonic metasurface for directional and frequency-selective thermal emission," Phys. Rev. Appl. **4**, 014023 (2015).
[27]J. A. Mason, S. Smith, and D. Wasserman, "Strong absorption and selective thermal emission from a mid-infrared metamaterial," Appl. Phys. Lett. **98**, 241105 (2011).
[28]E. Sakr and P. Bermel, "Thermophotovoltaics with spectral and angular selective doped-oxide thermal emitters," Opt. Express **25**, A880–A895 (2017).
[29]M. Garín, D. Hernández, T. Trifonov, and R. Alcubilla, "Three-dimensional metallo-dielectric selective thermal emitters with high-temperature stability for thermophotovoltaic applications," Sol. Energy Mater. Sol. Cells **134**, 22–28 (2015).
[30]X. Liu, Z. Li, Z. Wen, M. Wu, J. Lu, X. Chen, X. Zhao, T. Wang, R. Ji, Y. Zhang, L. Sun, B. Zhang, H. Xu, J. Zhou, J. Hao, S. Wang, X. Chen, N. Dai, W. Lu, and X. Shen, "Large-area, lithography-free, narrow-band and highly directional thermal emitter," Nanoscale **11**, 19742–19750 (2019).
[31]S. Campione, F. Marquier, J.-P. Hugonin, A. R. Ellis, J. F. Klem, M. B. Sinclair, and T. S. Luk, "Directional and monochromatic thermal emitter from epsilon-near-zero conditions in semiconductor hyperbolic metamaterials," Sci. Rep. **6**, 34746 (2016).
[32]J.-J. Greffet, R. Carminati, K. Joulain, J.-P. Mulet, S. Mainguy, and Y. Chen, "Coherent emission of light by thermal sources," Nature **416**, 61–64 (2002).
[33]S. E. Han and D. J. Norris, "Beaming thermal emission from hot metallic bull's eyes," Opt. Express **18**, 4829–4837 (2010).
[34]C. Arnold, F. M. C. Marquier, M. Garin, F. Pardo, S. Collin, N. Bardou, J.-L. Pelouard, and J.-J. Greffet, "Coherent thermal infrared emission by two-dimensional silicon carbide gratings," Phys. Rev. B **86**, 035316 (2012).
[35]M. De Zoysa, T. Asano, K. Mochizuki, A. Oskooi, T. Inoue, and S. Noda, "Conversion of broadband to narrowband thermal emission through energy recycling," Nat. Photonics **6**, 535–539 (2012).
[36]I. Celanovic, D. Perreault, and J. Kassakian, "Resonant-cavity enhanced thermal emission," Phys. Rev. B **72**, 075127 (2005).
[37]I. Celanovic, N. Jovanovic, and J. Kassakian, "Two-dimensional tungsten photonic crystals as selective thermal emitters," Appl. Phys. Lett. **92**, 193101 (2008).
[38]S. L. Chuang, *Physics of Photonic Devices*, 2nd ed. (John Wiley & Sons, Inc., 2009), pp. 1–821.
[39]S. Noda, K. Kitamura, T. Okino, D. Yasuda, and Y. Tanaka, "Photonic-crystal surface-emitting lasers: Review and introduction of modulated-photonic crystals," IEEE J. Sel. Top. Quantum Electron. **23**, 1–7 (2017).
[40]W. W. Chow, K. D. Choquette, M. H. Crawford, K. L. Lear, and G. R. Hadley, "Design, fabrication, and performance of infrared and visible vertical-cavity surface-emitting lasers," IEEE J. Quantum Electron. **33**, 1810–1824 (1997).
[41]M. Yoshida, M. De Zoysa, K. Ishizaki, Y. Tanaka, M. Kawasaki, R. Hatsuda, B. Song, J. Gelleta, and S. Noda, "Double-lattice photonic-crystal resonators enabling high-brightness semiconductor lasers with symmetric narrow-divergence beams," Nat. Mater. **18**, 121–128 (2019).
[42]T. Inoue, R. Morita, M. Yoshida, M. De Zoysa, Y. Tanaka, and S. Noda, "Comprehensive analysis of photonic-crystal surface-emitting lasers via time-dependent three-dimensional coupled-wave theory," Phys. Rev. B **99**, 035308 (2019).
[43]X. Huang, Y. Lai, Z. H. Hang, H. Zheng, and C. Chan, "Dirac cones induced by accidental degeneracy in photonic crystals and zero-refractive-index materials," Nat. Mater. **10**, 582–586 (2011).
[44]B. Zhen, C. W. Hsu, Y. Igarashi, L. Lu, I. Kaminer, A. Pick, S.-L. Chua, J. D. Joannopoulos, and M. Soljačić, "Spawning rings of exceptional points out of Dirac cones," Nature **525**, 354–358 (2015).
[45]K. Sakoda, "Proof of the universality of mode symmetries in creating photonic Dirac cones," Opt. Express **20**, 25181–25194 (2012).
[46]M. Minkov, I. A. D. Williamson, M. Xiao, and S. Fan, "Zero-index bound states in the continuum," Phys. Rev. Lett. **121**, 263901 (2018).
[47]S. Y. Chou, P. R. Krauss, W. Zhang, L. Guo, and L. Zhuang, "Sub-10 nm imprint lithography and applications," J. Vac. Sci. Technol. B **15**, 2897–2904 (1997).
[48]T. Inui, Y. Tanabe, and Y. Onodera, *Group Theory and Its Applications in Physics* (Springer Science & Business Media, 2012), Vol. 78.
[49]A. Y. Song, A. R. K. Kalapala, W. Zhou, and S. Fan, "First-principles simulation of photonic crystal surface-emitting lasers using rigorous coupled wave analysis," Appl. Phys. Lett. **113**, 041106 (2018).
[50]H. A. Haus, *Waves and Fields in Optoelectronics* (Prentice Hall, 1984), p. 402.
[51]W. Suh, Z. Wang, and S. Fan, "Temporal coupled-mode theory and the presence of non-orthogonal modes in lossless multimode cavities," IEEE J. Quantum Electron. **40**, 1511–1518 (2004).
[52]A. C. Overvig, S. C. Malek, M. J. Carter, S. Shrestha, and N. Yu, "Selection rules for quasibound states in the continuum," Phys. Rev. B **102**, 035434 (2020).
[53]Y. Xu, Y. Li, R. K. Lee, and A. Yariv, "Scattering-theory analysis of waveguide-resonator coupling," Phys. Rev. E **62**, 7389–7404 (2000).